Appl Phys B (2011) 105:231–237
DOI 10.1007/s00340-011-4662-5

Applied Physics B
Lasers and Optics

Investigation of plasmonics resonance infrared bowtie metal antenna

W. Zhong · Y. Wang · R. He · X. Zhou

Received: 24 January 2011 / Revised version: 19 May 2011 / Published online: 29 July 2011

Abstract An approximate resonance wavelength equation that varies with metal antenna structure size is developed to design a bowtie gold metal antenna working at near-infrared (IR) wavelength. Bowtie antenna structures with resonance wavelength of 1.06 μm, 1.55 μm and 10.6 μm are designed based on this equation. A finite-difference time domain (FDTD) algorithm with total field scattered field (TFSF) source simulation shows the resonance wavelength of the designed structures being precisely in agreement with the expected wavelengths from the equation. Planar integration of the metal bowtie antennas is discussed as well. Gold nanohole bowtie antenna arrays are fabricated and the near-field optical transmission properties of the nanohole array are investigated with a near-field scanning optical microscope (NSOM). Our experimental results verify the near-field optical transmission performance and further demonstrate that they are in agreement with the theoretical calculation results. The high enhancement efficiency and integration of the metal bowtie antennas open the possibility of a wide application in IR optoelectronics detection and imaging.

W. Zhong · Y. Wang · R. He · X. Zhou (✉)
School of Physical Electronics, University of Electronic Science and Technology of China, Chengdu 610054, Sichuan Province, P.R. China
e-mail: xiulizh@umich.edu

X. Zhou
Department of Electrical Engineering and Computer Science, University of Michigan, Ann Arbor, MI 48109, USA

1 Introduction

In recent years, metal antennas work at optical frequency present prospective applications in optoelectronics due to the localized surface plasmon resonance (LSPR) effects of metal nanoparticles, which induce large near-field enhancement and high far field irradiative efficiency [1–5]. Typical metallic nanoparticle's geometries such as spheres, cross-shaped Ag nanoparticles [6], rhombic plasmonic nanoparticle [7], disks [8], and bowties [9, 10] on a support substrate, e.g. quartz or glass, can exhibit resonances in the visible optical spectrum [11, 12], their optical properties and applications were explored and the high antennas emission characteristics of the particles are associated with the LSPR effects as well. Among the antennas with different structure characteristics, the bowtie metal antenna has stronger localized field distribution due to its confined geometry, which results in field enhancement at the sharp ends of the structure [13]. Gold has a strong SPR effect [14] and stable physical properties, it is a good candidate metal in infrared detector [5]. The electronic field distribution and intensity enhancement are discussed in many pioneers' work in visible and IR light range [3–5, 15–17]. However, still there is no a clear way to guide the designing of the bowtie antenna structure with an expecting resonant wavelength, and most of the discussions are on the single antenna cell and in visible wave range.

In this paper, the extinction and resonance properties of the single bowtie Au antenna work in near IR range with different sizes are investigated. A linear equation is deduced to approximately guide the designing of bowtie antenna resonant at a specific near IR wavelength. FDTD simulations confirmed the design and the integration discussion of the antennas are performed. Gold bowtie array is fabricated and the near-field transmission properties are investigated with

near-field scanning optical microscope (NSOM). It is observed that the experimental results are in agreement with the FDTD calculation results. The integrated IR antennas present a practical approach to open up its practical application ranging from IR optoelectronics detection to IR imaging.

2 Simulation environment and antenna modeling

In this paper, the simulations are based on commercial FDTD algorithm software presented by Lumerical Inc., named FDTD Solution. In the simulations of single bowtie antenna, the absorption boundary condition is adopted, and periodic condition is attached in the simulations of bowtie antenna array.

The schematic of the bowtie metal antenna is shown in Fig. 1, where the golden color area is the gold (Au) film, the gray etched area is air. In the simulation, the thickness of the Au is kept to be 0.1 μm, and the dielectric constant of the Au is referenced from Ref. [18] and fitted as described by Jensen [19]. This basic bowtie antenna cell structure is also used to analyze its integration.

Total field scattered field (TFSF) provided by FDTD Solution is introduced as the optical source to investigate the resonance properties of the single bowtie antenna structure. TFSF source is a useful light source for nanoparticle scattering problems. The TFSF source separates the simulation area into two regions: an interior region in which the total field, an incident plane wave plus the resulting scattered field is calculated, and an exterior region in which only the scattered field is calculated.

To explore the enhancement factor of the designed structure and the energy coupling among the bowtie metal antennas in the integration, plane wave source polarizing along y-direction is set to be the incident light at the resonance wavelength of the structure, since the electric field enhancement achieves its maximum at the resonance wavelength.

3 Optical properties and structure size design of the bowtie metal antenna

The structure parameters of the single bowtie metal antenna and the integration are shown in Figs. 1a–1b this planar integration structure is symmetrical both along x- and y-direction. The relationship of $L = W$ and $AL = (W - S)/2$ exist among the parameters. In our simulation work, we set $S = 0.2$ μm and $L = W$. With the help of TFSF source provided by FDTD Solution, we got the scattering, absorption and extinction properties of the designed bowtie antenna in near IR wavelength range, which are presented in Figs. 2a–2c. The spectra show the resonance peaks shift to longer wavelength with increasing the structure size of the bowtie antenna. It also shows the intensity enhancement ratio is increasing and the resonance spectra are broadened apparently.

The extinction resonance peaks in Fig. 2c were adopted to analyze the resonance characteristics vary with the structure size. Figure 2d shows the resonance wavelengths λ_R vary with the arm length AL. Their relations were plotted and fitting with MATLAB Tool software. The corresponding linear equation of the resonance wavelength vs. arm length is deduced as

$$y = 7.3 \times x + 1 \tag{1}$$

In this model, $y = \lambda_R$, $x = AL$. This equation helps to design the concrete bowtie Au antenna structure corresponding to a special near IR resonance wavelength. Considering an IR wavelength of 10.6 μm, $AL = 1.32$ μm is obtained with this equation. Figures 3a–3b presents the corresponding calculated extinction spectrum and the E-field intensity distribution at the emission surface of the designed bowtie antenna. The resonance wavelength of the designed bowtie antenna fits well with the expected resonance wavelength.

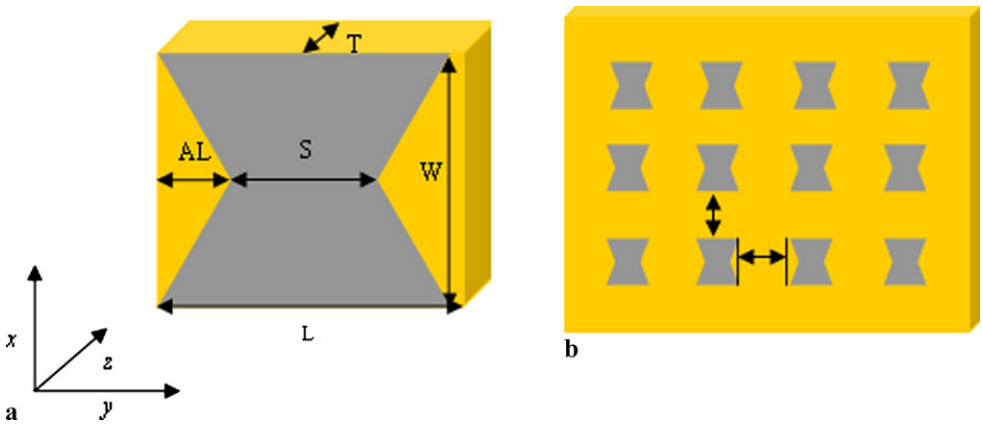

Fig. 1 (**a**) The schematic of single bowtie mental antenna. Where S, Al, L, W and T are the distances sign shown in the figure. (**b**) The schematic of the planar integration of bowtie metal antenna. The *arrows* denote the distance between the bowtie cells along x and y-direction

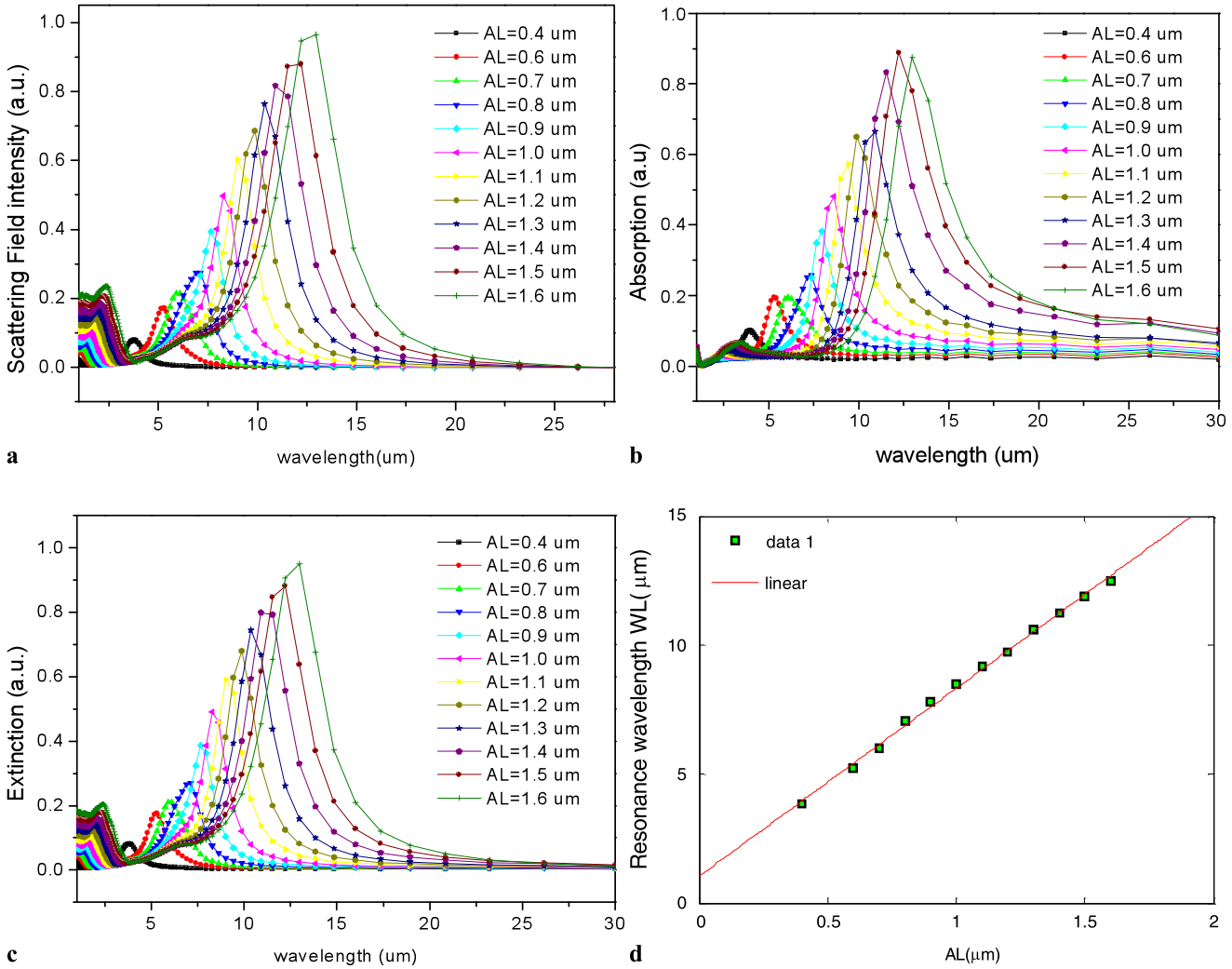

Fig. 2 (**a**) The scattering spectrum, (**b**) the absorption spectrum and (**c**) the extinction spectrum vary with the arm length *AL*. (**d**) The extinction resonance wavelength (*WL*) vs. the arm length *AL*

Fig. 3 (**a**) The scattering, absorption, and extinction spectrum of the designed bowtie antenna with resonance wavelength at 10.6 μm; (**b**) the E-field intensity distribution at the emission surface of the designed bowtie metal antenna with the incident wavelength of 10.6 μm. The *AL* of the antenna is 1.32 μm

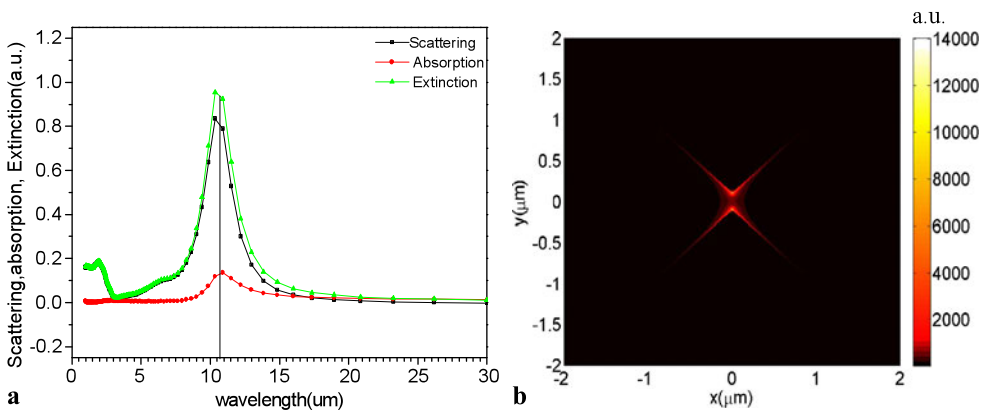

It shows this equation can guide the designing of a bowtie IR antenna which could be resonant at a specific IR wavelength. The E electric field intensity distribution in Fig. 3b shows the enhancement ratio is as high as $\sim 10^4$.

To further investigate the application on other IR wavelengths, the structure size of the near IR wavelength of 1.06 μm and 1.55 μm antenna are designed according to (1). The corresponding $AL = 0.01$ μm and 0.075 μm

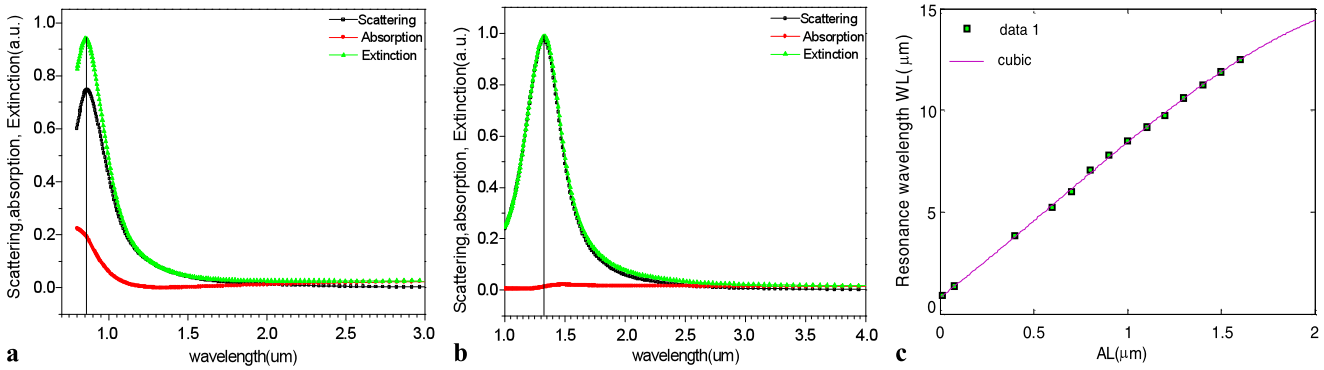

Fig. 4 The scattering, absorption, and extinction spectrum of the designed near IR bowtie metal antenna with the linear equation, with (**a**) $AL = 0.01$ μm (**b**) $AL = 0.075$ μm. the resonance peaks are at 0.86 μm and 1.33 μm. (**c**) The cubic fitting relation between resonant wavelength WL and arm length AL

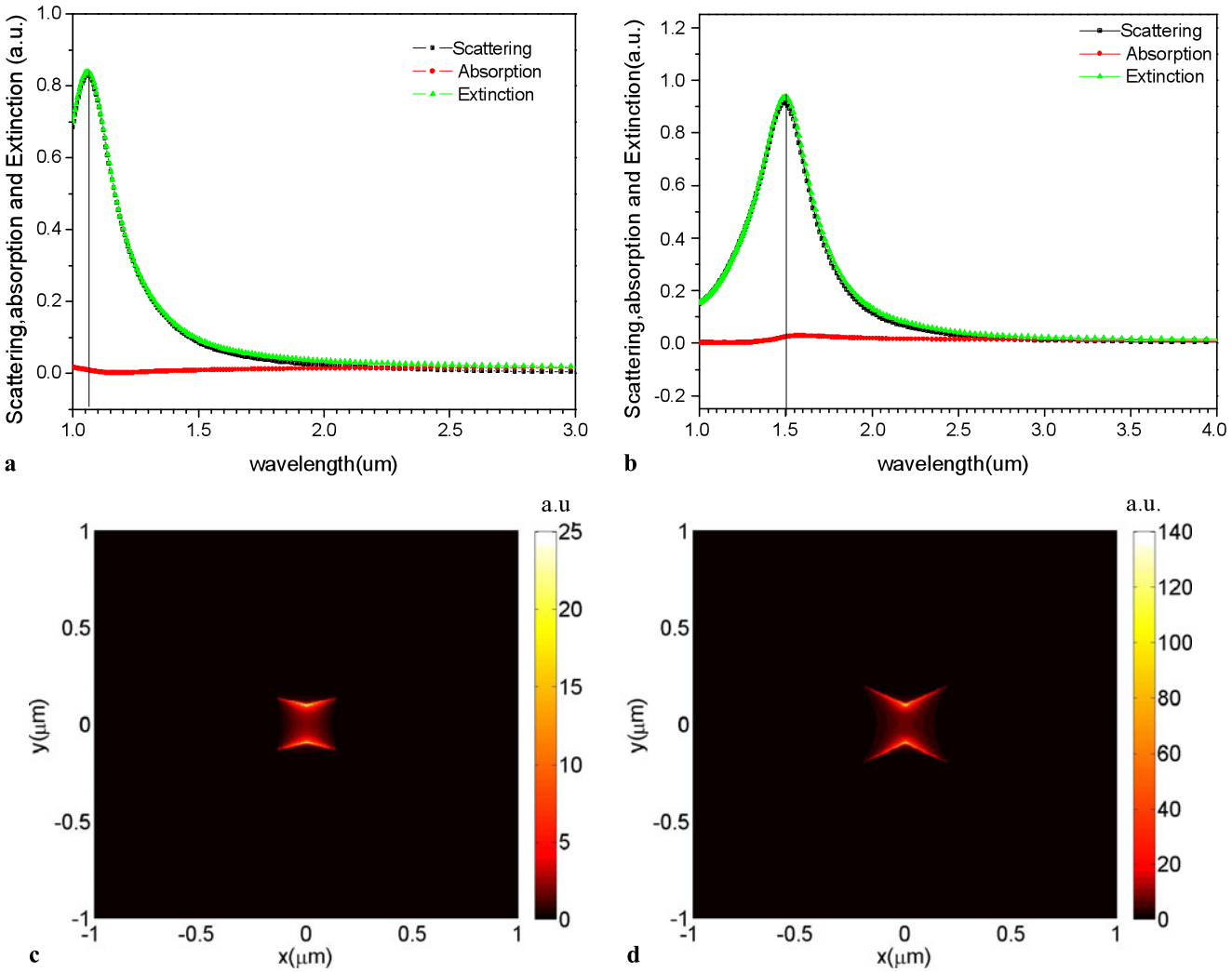

Fig. 5 The scattering, absorption, and extinction spectrum of the designed bowtie antenna with the modified equation, with (**a**) $AL = 0.035$ μm, (**b**) $AL = 0.1$ μm the resonance peaks are at 1.06 μm and 1.55 μm The corresponding E-field intensity distribution at the emission surface of bowtie antennas when the wavelength of source set to be the resonance wavelength of the antennas ((**c**) resonance wavelength of 1.06 μm; (**d**) resonance wavelength of 1.55 μm)

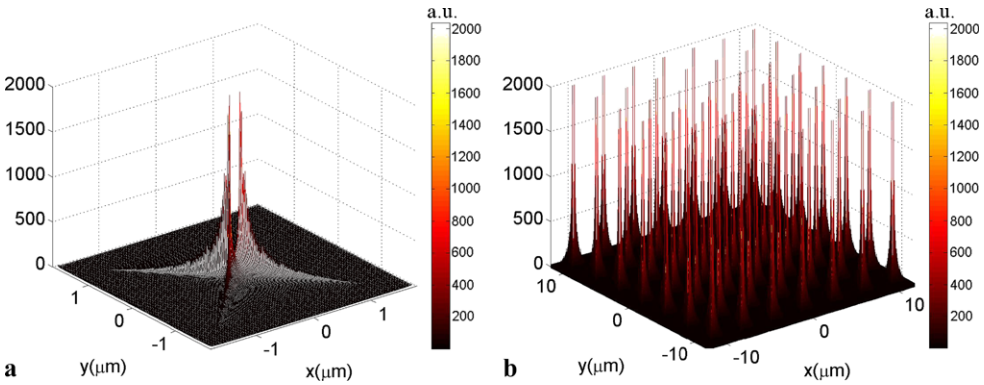

Fig. 6 (**a**) The calculated E-field intensity distribution of bowtie Au antenna working at 10.6 μm. (**b**) The calculated E-field intensity distribution of the planar integration bowtie Au antenna with periodic boundary condition

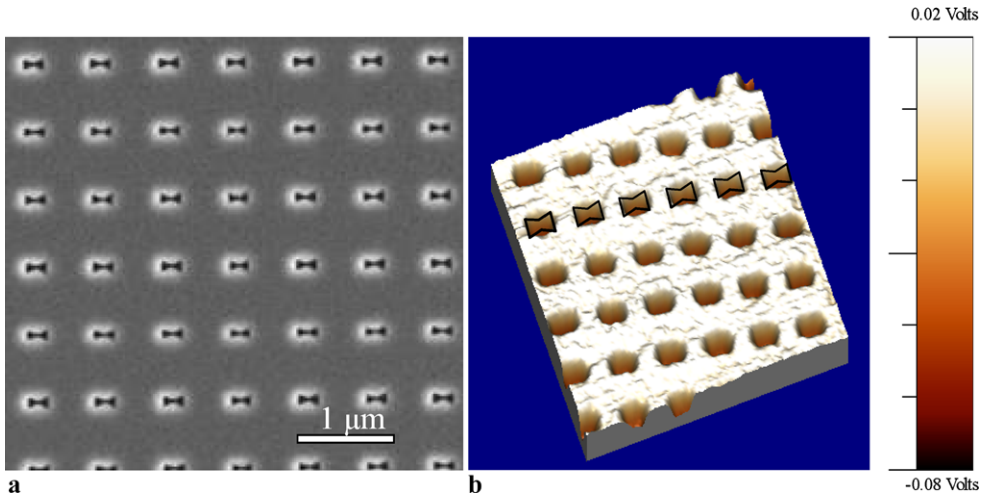

Fig. 7 The SEM and AFM measured topography image of the nanohole bowtie antenna array

are obtained, and the extinction spectra are shown in Figs. 4a–4b.

Figure 4a–4b show the resonance wavelengths are diverged to ∼0.86 μm and ∼1.33 μm, respectively. Considering the shorter IR wavelength scope, a higher order equation based on previous (1) is deduced as

$$y = -0.68 \times x^3 + 1.2 \times x^2 + 7.1 \times x + 0.82 \qquad (2)$$

Here resonance wavelength λ_R is denoted as y and arm length AL is denoted as x. This new equation is also fitted with MATLAB Tool software. And in longer IR wavelength scope, it is equivalent to the linear (1). The data and fitting curve are presented in Fig. 4c.

To the resonance wavelength of 1.06 μm and 1.55 μm, $AL = 0.035$ μm and 0.1 μm are obtained with this new equation. FDTD calculation based on the new size is shown as Figs. 5a–5b. It is shown that the resonance wavelength of this new model is as expected as 1.06 μm and 1.55 μm, respectively. And the enhanced electric intensity distribution at the emission surface of the structure is shown as Figs. 5c–5d, which motivates a potential application in IR photoelectronic detection.

4 The investigation of the bowtie metal antenna integration

Planar integration technology is an essential approach to open up the potential application of the designed bowtie antenna working at a specific IR wavelength.

Figure 6 further demonstrates a three dimensional E-field distribution obtained with periodical boundary condition. It works at 10.6 μm. The large area antenna pattern shows a strong E-field distribution which motivates a prospective application in IR imaging.

Nanohole bowtie arrays are fabricated using focused ion beam (FEI Quanta 200 3D dual beam system) directly milling technique and NSOM (MultiView 2000^{TS} from Nanonics Inc. in Israel) is employed. It can perform both an Atomic Force Microscope (AFM) Scanning and a NSOM Scanning. The Scanning Electronic Microscope (SEM) and AFM image of the bowtie antenna array is shown as Fig. 7. To get the optical transmission properties through the nanohole bowtie arrays, a tapered single mode fiber probe working in collection mode is used. The aperture diameter of the fiber probe is 150 nm and the working wavelength of the light source is 532 nm (Nd:YAG laser with

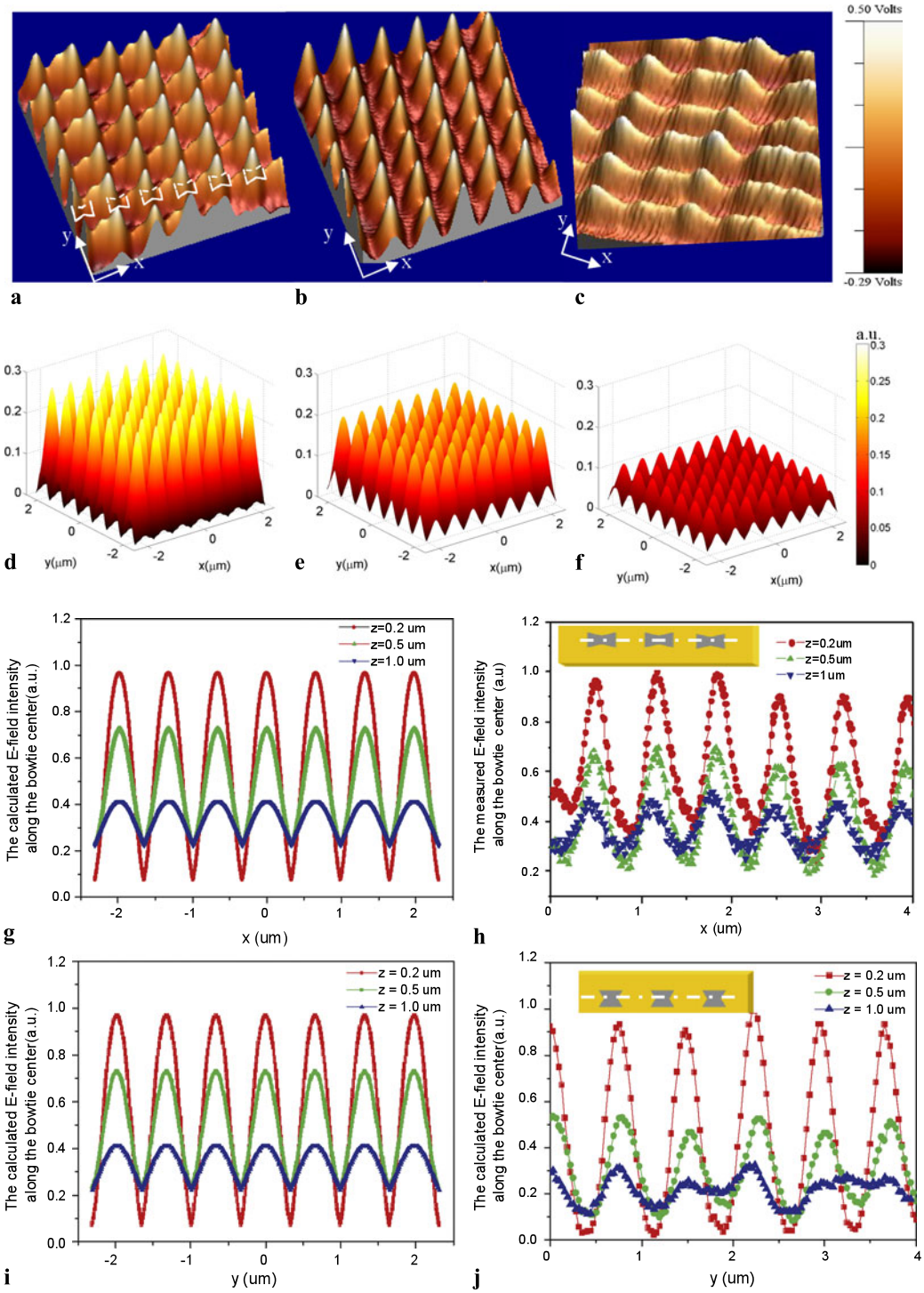

Fig. 8 NSOM measured E-field intensity distribution at x–y plane with a propagation distance of (**a**) $z = 200$ nm, (**b**) $z = 500$ nm and (**c**) $z = 1000$ nm from the exit surface of the nanohole bowtie array, respectively. And the calculated E-field intensity distribution of the nanohole bowtie antenna array with the E-field distribution at the height of (**d**) $z = 200$ nm, (**e**) $z = 500$ and (**f**) $z = 1000$ from the sample surface, respectively. The simulation model is in accordance with the experimental model in (**a**, **b** and **c**), but with periodic boundary condition. (**g**–**h**) and (**i**–**j**) show the comparison of the normalized measured and calculated E-intensity distribution along the center of the nanohole bowtie antenna. (**g**) Measured curves of x-direction along the center of the bowtie antenna, the curves are corresponding to the measured positions at 200 nm, 500 nm and 1000 nm from the exit surface of the nanohole array; (**h**) calculated results of x-direction along the center of the bowtie antenna, the curves are corresponding to the perpendicular transmission positions at 200 nm, 500 nm, and 1000 nm from the exit surface. (**i**) Measured curves of y-direction along the center of the bowtie antenna, the curves are corresponding to the measured positions at 200 nm, 500 nm and 1000 nm from the exit surface of the nanohole array; (**j**) calculated results of y-direction along the center of the bowtie antenna, the curves are corresponding to the perpendicular transmission positions at 200 nm, 500 nm, and 1000 nm from the exit surface

power of 20 mW). Firstly, the tip was scanning close to the sample surface. Then the fiber tip was raster scanned at a constant height of 200 nm, 500 nm, and 1000 nm above the sample surface, respectively. The optical intensity distribution of the transmitted light at different planes was mapped over a grid of 256 × 256 spanning an area of 4 μm × 4 μm.

The E-field distribution obtained by the NSOM is presented in Figs. 8a–8c. The transmission E-field intensities are decaying with the transmission distances increasing from the exit surface of the nanohole array. A simulation model is built corresponding to the experimental model, also with an incident light source with a wavelength of 532 nm. Figures 8d–8f shows the calculated three dimensional E-field results which show a good agreement with the experiment results shown in Figs. 8a–8c. Still the intensity distributions between the experimental and calculated results show a little difference. In the simulation model, a periodic condition is attached in the simulations of bowtie antenna array. No coupling effects among the bowtie antennas are presented in Figs. 8d–8f. On the contrary, the experimental results show a non-symmetrical E-field distribution because of the no-symmetrical structure of the bowtie antenna and coupling effects among the antennas. Especially in Fig. 8c, it show a near continuous E-intensity distribution along the x-direction. Both the experimental and calculation results show strong E-field intensity distribution at the center area of the bowtie antenna.

Figures 8(h) and 8(j) present the normalized measured E-field intensities distribution along the center of the bowtie antennas at different scanning height from the surface of the array. They are in agreement with the calculated normalized intensity distributions as shown in Figs. 8(g) and 8(i). The inset pictures in Figs. 8(h) and 8(j) show the cross-section positions along x and y-directions of the bowtie antennas.

5 Conclusion

TFSF source and FDTD algorithm are used to investigate the optical properties of the bowtie metal antenna. An approximate resonance wavelength vs. structure size equation is developed to design the bowtie gold antenna working at specific near-infrared (IR) wavelength. Bowtie antenna structures with resonance wavelengths of 1.06 μm, 1.55 μm and 10.6 μm are designed based on this equation. FDTD with total field scattered field source simulation verified the resonance wavelength vs. the structure size equation. Planar integration of the metal bowtie antennas is discussed as well. Nanohole bowtie antenna array is fabricated in gold thin film supported on quartz substrate. The geometric characterization was performed using AFM, and the optical properties are characterized using NSOM. The NSOM images show the high E-field distribution near the surface of the Au film etched with a nanoholes array. FDTD algorithm is used to carry on studying the optical transmission property as well. Comparing the NSOM experimental results to the FDTD theoretical calculating results, the experimental results demonstrate that the measured transmission results are in agreement with the calculated results. The high enhancement efficiency and integration of the metal bowtie antennas motivate a wide application in IR optoelectronic detection and imaging.

Acknowledgements This work is supported by "the Fundamental Research Funds for the Central Universities", under Grant No. ZYGX2010J053.

References

1. P.J. Schuck, D.P. Fromm, A. Sundaramurthy, G.S. Kino, W.E. Moerner, Phys. Rev. Lett. **94**, 017402 (2005)
2. P. Muhlschlegel, H.J. Eisler, O.J.F. Martin, B. Hecht, D.W. Pohl, Science **308**, 1607 (2005)
3. V.B. Svetlana, D.N. Luca, Opt. Lett. **35**, 538 (2010)
4. P.K. Jain, K.S. Lee, I.H. El-Sayed, M.A. El-Sayed, J. Phys. Chem. B **110**, 7238 (2006)
5. H. Guo, P.M. Todd, Z. Thomas, L. Na, L. Fu, S. Heinz, G. Harald, Opt. Express **16**, 7756 (2008)
6. M. Zhang, X. Zhou, Y. Fu, Plasmonics. doi:10.1007/s11468-010-9150-y (2010)
7. X. Zhou, M. Zhang, L. Yi, Y. Fu, Plasmonics. doi:10.1007/s11468-010-9173-4 (2010)
8. Z. Liu, A. Boltasseva, R.H. Pedersen, R. Bakker, A.V. Kildishev, V. Drachev, V.M. Shalaev, Metamaterials **2**, 45 (2008)
9. H. Fischer, O.J.F. Martin, Opt. Express **16**, 9144 (2008)
10. D.P. Fromm, A. Sundaramurthy, P.J. Schuck, G. Kino, W.E. Moerner, Nano Lett. **4**, 957 (2004)
11. W. Rechberger, A. Hohenau, A. Leitner, J.R. Krenn, B. Lamprecht, F.R. Aussenegg, Opt. Commun. **220**, 137 (2003)
12. T. Atay, J.H. Song, A.V. Nurmikko, Nano Lett. **4**, 1627 (2004)
13. X. Jiao, G. Jeremy, S. Blair, OSA technical digest (CD), Optical Society of America, paper JWD41 (2008)
14. D. Gérard, J. Wenger, N. Bonod, E. Popov, H. Rigneault, F. Mahdavi, S. Blair, J. Dintinger, T.W. Ebbesen, Phys. Rev. B **77**, 045413 (2008)
15. H. Li, X. Cheng, J. Vac. Sci. Technol. B **26**, 2156 (2008)
16. J. Alda, J.M. Rico-García, J.M. López-Alonso, G. Boreman, Nanotechnology **16**, S230 (2005)
17. A. Sundaramurthy, P.J. Schuck, N.R. Conley, D.P. Fromm, G.S. Kino, W.E. Moerner, Nano Lett. **6**, 355 (2006)
18. E.D. Palik, *Handbook of Optical Constants of Solids* (Academic Press, New York, 1985)
19. C.F. Bohren, D.R. Huffman, *Absorption and Scattering of Light by Small Particles* (Wiley, New York, 1983)